THE JOURNAL OF PHYSICAL CHEMISTRY B

Article

pubs.acs.org/JPCB

Raman and ROA Spectra of (−)- and (+)-2-Br-Hexahelicene: Experimental and DFT Studies of a π-Conjugated Chiral System

Christian Johannessen,[†] Ewan W. Blanch,[†] Claudio Villani,[‡] Sergio Abbate,*[,§,∥] Giovanna Longhi,[§,∥] Nisha R. Agarwal,[⊥,#] Matteo Tommasini,*[,⊥,#] and David A. Lightner[○]

[†]Faculty of Life Sciences and Manchester Institute of Biotechnology, John Garside Building, University of Manchester, 131 Princess Street, Manchester M1 7DN, U.K.

[‡]Dipartimento di Chimica e Tecnologia del Farmaco, Università degli Studi "La Sapienza", P.le Aldo Moro 5, 00185 Roma, Italy

[§]Dipartimento di Scienze Biomediche e Biotecnologie, Università di Brescia, Viale Europa 11, 25123 Brescia, Italy

[∥]CNISM Consorzio Interuniversitario per le Scienze Fisiche della Materia, Via della Vasca Navale, 84, 00146 Roma, Italy

[⊥]Dipartimento di Chimica, Materiali e Ingegneria Chimica "G. Natta" − Politecnico di Milano, Piazza Leonardo da Vinci 32, 20133 Milano, Italy

[#]Consorzio Interuniversitario per la Scienza e Tecnologia dei Materiali (INSTM), Unità di Ricerca del Politecnico di Milano (Dip. CMIC), Piazza Leonardo da Vinci 32, 20133 Milano, Italy

[○]Department of Chemistry, University of Nevada, Reno, Nevada 89557, United States

Supporting Information

ABSTRACT: The Raman optical activity (ROA) spectra of both enantiomers of 2-Br-hexahelicene in chloroform solution have been measured in the range 1700−300 cm^{-1}. Density functional theory (DFT) calculations accurately reproduce the observed features. The most intense ROA features are also the most intense Raman features, in the region 1350−1400 cm^{-1}, and correspond to the so-called D-modes, which play a major role in coronene and other PAHs (polycyclic aromatic hydrocarbons). Together with a detailed analysis of the normal mode structure, the polarizability tensors for the intense Raman features are investigated and related to the principal characteristics of helicene systems, namely, chirality and π-conjugation. Through electron−phonon coupling analysis, we propose a mechanism that justifies the intense ROA signals.

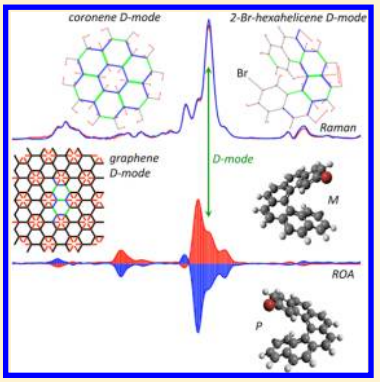

INTRODUCTION

Hexahelicenes are a group of molecules that combine applicative usefulness and theoretical importance. The former aspect is presently of upmost interest, with the rebirth of helicene studies, encompassing investigations of helicenes of various lengths and with various substituents for which several photonics and biosensing applications as well as interesting chirality-driven aggregation phenomena have been observed.[1−9] However, in this article, we are more interested in the second aspect that implies two intertwined aspects, chirality and π-conjugation, both of which are distinctly considered below for ease of discussion.

Chirality. Since the beginning of optical activity studies, hexahelicene has served to propose one of the first applications of the linear combination of atomic orbitals (LCAO) approach to defining molecular orbitals (MOs) and the first meaningful calculations of optical rotation (OR)[10,11] through the celebrated Rosenfeld formula.[12] Furthermore, due to its inherently chiral molecular structure, hexahelicene served as an exemplary molecule to formulate the theory encompassing Rayleigh optical activity[13] and optical rotation.[14] Subsequently, the assignment of the absolute configuration (AC) of hexahelicene was unequivocally established on the basis of the combined use of OR, of electronic circular dichroism (ECD) and of X-ray diffraction methods, in a comparative investigation of (+) and (−)-hexahelicene, (+) and (−)-2-Br-hexahelicene, and (+) and (−)-2-CH_3-hexahelicene[15,16] (in all cases, the (−) optical isomer was found to be associated with the *M* helicity). The latter study pointed out that an erroneous prediction of AC had been made in refs 10 and 11. Progress in *ab initio* methods and use of more powerful computational routines allowed identification of the origin of the inadequacy of the first theoretical attempt[17,18] as the lack of diffuse atomic orbitals.

Recently, the AC of 2-Br-hexalicene was confirmed by vibrational circular dichroism (VCD) and density functional theory (DFT) calculations.[19] VCD is one of the two forms of

Received: December 17, 2012
Revised: January 21, 2013
Published: January 23, 2013

 © 2013 American Chemical Society dx.doi.org/10.1021/jp312425m | J. Phys. Chem. B 2013, 117, 2221−2230

vibrational optical activity (VOA), which also encompasses Raman optical activity (ROA).[20−23]

Here, we complete the VOA analysis of 2-Br-hexahelicene, by reporting the Raman and ROA spectra of the molecule. There are several motivations to the present investigation: We wish to inquire whether there is a complementarity in the information from VCD and ROA, inasmuch as there is a complementarity in the IR and Raman spectra of the same molecule. Concurrently, we wish to learn whether the normal modes (NM) exhibiting strong Raman and ROA bands and the NM corresponding to strong IR and VCD bands bear some analogy in terms of their "geometrical" and "electrical" behavior.

The ROA experiments have been performed in the so-called scattered circular polarization (SCP) approach in the back-scattering geometry, which allows simultaneous measurements of the Raman scattered circularly polarized components with intensities I^R and I^L that are related to fundamental molecular quantities through the following relations:[20−23]

$$I^R - I^L = \frac{8K}{c}[12\beta(G')^2 + 4\beta(A)^2] \quad (1)$$

$$I^R + I^L = 4K[45\bar{\alpha}^2 + 7\beta(\alpha)^2] \quad (2)$$

In eqs 1 and 2, α, G', and A are the vibrational transition moments of quantities defined respectively by the real part of the products of the electric dipole−electric dipole (polarizability tensor) $\boldsymbol{\alpha}$, by the imaginary part of the electric dipole−magnetic dipole tensor $\mathbf{G}'$, and by the real part of the traceless electric dipole−electric quadrupole tensor $\mathbf{A}$.[20,24] In eq 2, $\bar{\alpha}$ represents the invariant mean polarizability derivative (one-third the trace of $\boldsymbol{\alpha}$) and β is the invariant anisotropy of the various tensors involved in the Raman and ROA phenomena. K is a constant associated with the scattering of radiation, and c is the speed of light. Importantly, the same $\mathbf{G}'$ tensor at vibrational equilibrium can be found in the expression of the optical rotation, namely,[22,25]

$$\phi = -\frac{1}{3}\omega\mu_0 L{\cdot}N(G'_{xx} + G'_{yy} + G'_{zz}) \quad (3)$$

In eq 3, L, ω, and μ_0 are, respectively, the cell length, radiation angular frequency, and magnetic permeability constant, while N is the Avogadro constant. Through eq 3, Polavarapu[26,27] was able to derive the first proposal on how to calculate OR by modern *ab initio* methods, which elegantly illustrates how the ROA and OR phenomena are related. It is well-known that the specific OR of hexahelicene is extraordinarily large; for example, in 2-Br-hexahelicene, it is close to 4000.[15,16] Thus, we may expect the ROA intensities of hexahelicene to be similarly large, since the latter observable, by eq 1, is determined by a characteristic of the very same $\mathbf{G}'$ tensor, as explicitly exploited in *ab initio* calculations of OR.[28,29]

π-Conjugation. All helicene systems are constituted by ortho-fused benzene molecules, each aromatic unit having a large polarizability tensor, with cylindrical symmetry and thus with two independent parameters: The in-plane $\alpha_\parallel$ polarizability is approximately equal to 12 Å^3, and the orthogonal $\alpha_\perp$ polarizability is close to 6 Å^3.[30−32] The latter values are rather large, and due to this, we can also expect strong Raman features, at least for some vibrational NM. It is also interesting to note that Barron, co-workers, and the British school devoted much work and numerous papers to establishing a relation between group (bond) polarizabilities and $\mathbf{G}'$ and $\mathbf{A}$ tensors.[22,23,33−35]

For a better characterization of the NMs contributing to ROA and Raman spectra and to shed light on the vibrational structure of 2-Br-hexahelicene, we have decided to complete the present work by including the IR and Raman spectra of the molecule down to 400 cm^{-1}, in solution and the solid phase, in order to examine differences in the spectra of solution vs solid samples.

Similarly to the case of other π-conjugated systems,[36] we believe that the present studies will be helpful for applications in nonlinear optics. Indeed, a Raman optical activity study is most appropriate for this group of molecules, as they possess large second-order susceptibilities,[37] due to inherent chirality and yet high π-conjugation: For this reason, they are prone to be used, e.g., in designing three-wave-mixing devices. Furthermore, since oligoenes and polycyclic aromatic hydrocarbons (PAH) serve as molecular models to understand the Raman response of related π-conjugated systems, such as polyacetylene and graphene,[38] we envisage that helicenes may well serve as prototypes to explore the possible ROA response of chiral systems based on graphene; see, for instance, ref 39. For this reason, a preliminary DFT investigation of the polarizability tensor will be given here.

EXPERIMENTAL SECTION

Synthesis and Enantiomer Separation. The synthesis of 2-Br-hexahelicene was carried out in the University of California (Los Angeles) laboratories and is described in refs 15 and 16. Initiating this study, only the racemic mixture was available and so a new enantiomeric HPLC separation had to be performed to produce a sample in enough quantity to carry out ROA experiments, the details of which are presented below:

Experimental Apparatus. Analytical liquid chromatography was performed on a JASCO chromatograph equipped with a Rheodyne model 7725i 20 μL injector, PU-1580-CO2 and PU-980-HPLC pumps, a Mod Jasco-975 single wavelength absorbance detector, and a Jasco Mod 995-CD circular dichroism detector. Chromatographic data were collected and processed using Borwin software (Jasco Europe, Italy). Semipreparative liquid chromatography was performed on a Waters chromatograph (Waters Associates) equipped with a Rheodyne model 7012 200 μL loop injector, a UV SpectraMonitor 4100 spectrophotometer, and a refractive index Waters R401 detector.

Chromatographic Procedures. The enantiomers of 2-Br-hexahelicene were resolved by semipreparative HPLC using a Chiralpak-IB column (250 × 10 mm I.D.), *n*-hexane/dichloromethane 95/5 as eluent (flow rate 5 mL/min and T = 25 °C), and UV detection at 280 nm. The sample was dissolved in a chloroform/mobile phase 60/40 (c = 12 mg/mL), and 200 μL (2.4 mg) was injected each run (process yield 95%). The enantiomeric excess of the collected fractions was checked by analytical HPLC using a Chiralpak-IB column (250 × 4.6 mm I.D.) under the same conditions employed for the semipreparative mode, except for the flow rate (1 mL/min). For each enantiomer, we obtained 17 mg with e.e. = 98.9% (1st eluted) and 98.7% (2nd eluted) (see Figure SI-1, Supporting Information, for further details). Polarimetric measurements on the first eluted enantiomer gave $[\alpha]_D^{25}$ = −3788 (c 0.049, $CHCl_3$) This value is close to those reported in ref 16.

ROA Measurements. Samples of enantiomerically pure 2-Br-hexahelicene were dissolved in HPLC grade chloroform at a concentration of 0.030 M and subsequently loaded into quartz microfluorescence cells. Raman and ROA measurements were

performed using a ChiralRAMAN instrument (Biotools, Jupiter, FL), engineered according to Hug's design,[40] with the following experimental conditions: laser excitation wavelength 532 nm; laser power at the sample ~100 mW; spectral resolution ~7 cm^{-1}; acquisition time 12 h. Solvent chloroform spectra were subtracted from the parent Raman spectra, and the ROA spectra were smoothed using a five-point FTT filter.

FT-Raman and IR Measurements. *FT-Raman.* Solid samples of both racemic and enantiomerically pure 2-Br-hexahelicene were measured as received from chemical synthesis or enantiomer separation steps. FT-Raman spectra of 2-Br-hexahelicene in CH_2Cl_2 solution state were acquired at 0.0285 M concentration. FT-Raman Nicolet NXR9650 equipment was used, with Nd-YVO_4 laser excitation at 1064 nm, a Peltier cooled InGaAs detector, and a spectral resolution of 4 cm^{-1}. Unpolarized Raman scattering was recorded in the backscattering geometry. Within experimental noise, and as expected, we did not notice any difference between the spectra of the two enantiomers or the racemate in the solid state in the FT-Raman experiments. This signifies that the two enantiomers and racemate do not exhibit significantly different packing motifs in the solid phase.

IR. Solid state infrared absorption was measured using the KBr pellet technique on the same enantiomerically pure samples also employed for solution state IR measurements in chloroform ($CHCl_3$). These experiments were carried out with an FT-IR Nicolet Magna 560 interferometer equipped with a DTGS detector. The spectral resolution was set to 1 cm^{-1}.

DFT Calculations. Density functional calculations were carried out with the Gaussian 09 program suite,[41] adopting the B3LYP functional and a triple-ζ basis set including polarization functions (TZVP). The choice of this method proved to be accurate in modeling the VCD response of 2-Br-hexahelicene.[19] Our results also compare favorably with previous theoretical investigations on hexahelicene.[42,43] Spectra have been simulated as a superposition of Lorentzian functions centered at the computed vibrational wavenumbers and with area proportional to the intensities (IR, Raman, ROA) determined by DFT calculations. The Lorentzian line width was assumed equal to 10 cm^{-1}. The DFT response calculation of ROA intensities was carried out assuming a finite excitation wavelength, fixed at an experimental value of 532 nm. For comparison with off-resonance FT-Raman spectra of 2-Br-hexahelicene, the static approximation was adopted in the DFT calculation of the Raman response (i.e., $\lambda_{exc} \rightarrow \infty$). In-house custom codes have been developed and used for the analysis and graphical representation of the vibrational normal modes.

RESULTS AND DISCUSSION

The results of the Raman and ROA experiments for both enantiomers of 2-Br-hexahelicene, compared to the predicted Raman and ROA spectra of the *P* enantiomer, are presented in Figures 1 and 2, in the regions 1800−800 and 650−375 cm^{-1}, respectively, omitting the strong chloroform bands between 800 and 700 cm^{-1}. In Figure SI-2 (Supporting Information), we provide the ball-and-stick representation of the *P* enantiomer of 2-Br-hexahelicene. While the Raman spectra of the enantiomeric pair are identical, the ROA spectra exhibit nearly perfect mirror image appearance and the predicted spectra are in excellent agreement with experiment, both for the ROA and the Raman data. One may notice that there are two major ROA bands: the first extending between 1350 and 1400 cm^{-1} and the second at ca. 410 cm^{-1}.

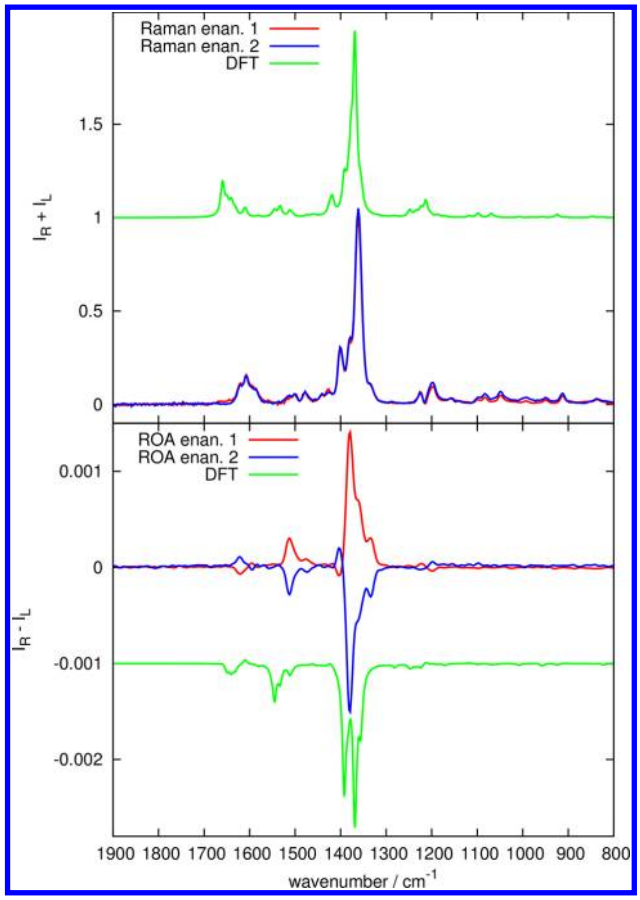

Figure 1. Experimental Raman (top) and ROA (bottom) of the two enantiomers of 2-Br-hexahelicene in $CHCl_3$. DFT calculations of Raman/ROA are for the *P* enantiomer (molecule in vacuo). The intensity scale has been normalized to the strongest Raman peak. For clarity, spectra simulated with DFT have been offset.

The observation of intense ROA bands is not unprecedented; indeed, in ref 44, a number of strong ROA bands have been reported. What is interesting and new in this case is that the strong ROA signal between 1350 and 1400 cm^{-1} is accompanied by an equally strong Raman signal. Still, the 1350 cm^{-1} ROA band has a CID dissymmetry factor close to 2×10^{-3}, an order of magnitude larger than average CID values, while the 410 cm^{-1} band has a CID close to 10^{-4}. Similar CID ratios are observed for more common molecules, frequently used as standards to calibrate spectra, like, e.g., pinenes and pinanes.[20−23,45] However, DFT calculations of the ROA signals of 2-Br-hexahelicene and of α- and β-pinene strikingly show that in order to display the ROA spectra of the pinenes on the same scale as the ROA of 2-Br-hexahelicene one has to magnify the spectra of the pinenes by a factor of 100 (see the Supporting Information, Figure SI-3).

Given that 2-Br-hexahelicene has Raman and ROA spectra exhibiting strong features, and since the electronic excitation energies of the pinenes lie well within the UV region (ca. 200 nm[46]), while 2-Br-hexahelicene absorbs at longer wavelengths,[16,19] a concern was raised about the intense Raman and ROA features not being due to an intrinsic effect but rather to a preresonance condition. Two facts have to be considered to this respect: (1) The off-resonance calculations reported above and presented in the Supporting Information are well in accord with experimental data. Indeed, Figure SI-3 of the

dx.doi.org/10.1021/jp312425m | J. Phys. Chem. B 2013, 117, 2221−2230

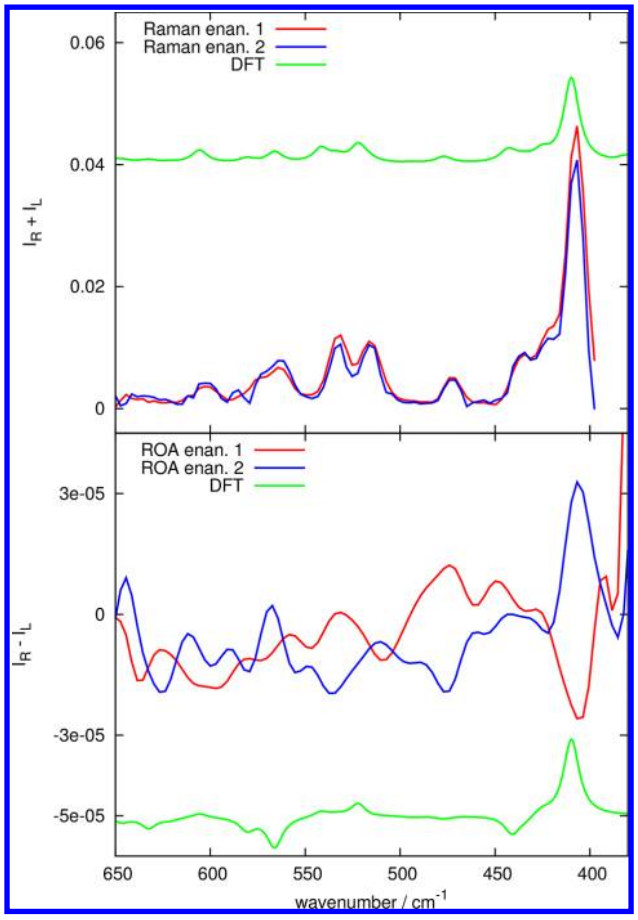

Figure 2. Experimental Raman (top) and ROA (bottom) of the two enantiomers of 2-Br-hexahelicene in $CHCl_3$. DFT calculations (green line) are for the *P* enantiomer (in vacuo). The intensity scale is the same as that for Figure 1.

Supporting Information provides evidence that the ROA of 2-Br-hexahelicene is always about 2 orders of magnitude larger than that of the pinenes, even in a hypothetical far-from-resonance condition (i.e., using 785 and 1064 nm excitations); however, we notice that excitation wavelength dependence is more pronounced for helicene than for pinene, thus suggesting the possible onset of preresonance phenomena. (2) The lowest electronic excitations of 2-Br-hexahelicene are found, both experimentally and by TD-DFT calculations, to be well separated in energy with respect to our 532 nm excitation, which is consistent with the results of refs 16 and 19, as the highest wavelength absorption is below 400 nm.

DFT calculations may provide some hints as to the meaning of the modes behind intense ROA and Raman bands. This aspect has been discussed thoroughly for simple hexahelicene by Liégeois and Champagne.[42] We simply reiterate it here due to the presence of the bromine atom. A relevant work to the concepts discussed in the present investigation is the theoretical analysis of strong ROA modes that has been provided by Luber and Reiher.[47]

Another recent interesting study based on DFT calculations[43] showed the strong similarities between the Raman responses of coronene and hexahelicene. Similarities are also evident in our theoretical results reported in Figure 3 and allow one to extend the molecular approach derived for the description of the Raman signals of graphitic materials[38] to helicenes as well. In fact, the Raman G- and D-lines found in

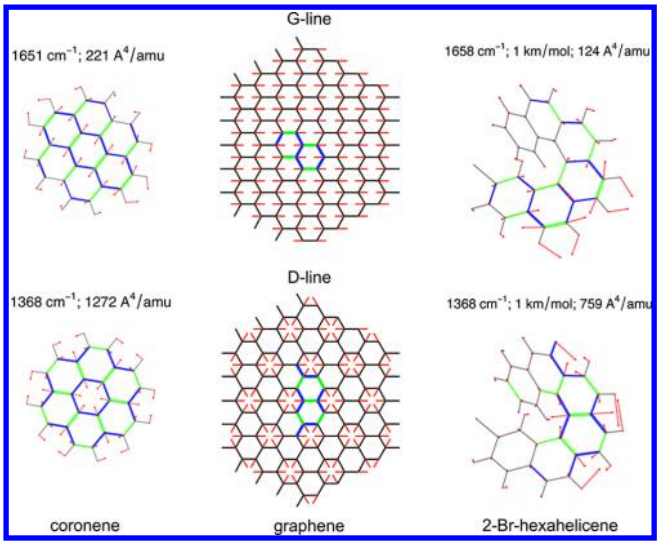

Figure 3. Sketch of selected nuclear displacements obtained from DFT calculations for the G and D lines in coronone (left) and 2-Br-hexahelicene (right). In the middle, the infinite case of graphene is depicted.[38] Red arrows represent displacement vectors; CC bonds are represented as green (blue) lines of different thickness according to their relative stretching (shrinking). DFT calculations are for the *P* enantiomer of 2-Br-hexahelicene.

graphenes are associated to vibrational NMs with characteristic nuclear displacement patterns[38] that are found in 2-Br-hexahelicene (see Figure 3) and that are also responsible for the peculiar selective behavior of the Raman spectrum in the equivalent G and D spectral regions in 2-Br-hexahelicene, at ca. 1600 and 1350 cm^{-1}, respectively (see Figure 1).

The description of NMs, derived on the basis of a custom code coupled to the outputs from a widely used quantum chemistry package,[41] is provided in Table 1 and Figure 4 for a selected number of relevant NMs. Three classes of modes in the region 1300−1700 cm^{-1} are discussed here.

Table 1. Synopsis of the Normal Modes of 2-Br-Hexahelicene Most Relevant for This Work (DFT, Unscaled Frequencies, *P* Enantiomer)

mode no.	frequency (cm^{-1})	spectroscopic characteristics	NM description
98	1552	VCD (−, P)	collective CC stretching, in-plane CH bending
96	1532	VCD (+, P)	collective CC stretching, in-plane CH bending
104	1658	ROA, Raman	ring stretching (G-type)
85	1368	ROA, Raman	ring breathing (D-type)
18	410	ROA, Raman	collective breathing
66	1098	IR (weak)	C−Br stretching
51	862	IR (strong)	collective CH out-of-plane

Two strong VCD modes (also IR active) are predicted[19] at 1552 and 1532 cm^{-1}: these modes comprise the second-strongest set of six ROA modes, the strongest one being calculated at 1545 cm^{-1} and their Raman intensity being not so large (see Table SI-1, Supporting Information), The set of NMs with largest ROA and Raman simultaneously are predicted in a region between 1354 and 1392 cm^{-1}, the strongest one being at 1368 cm^{-1} (D-modes, see Table SI-1, Supporting Information). The second strongest set of Raman modes are predicted at ca. 1650 cm^{-1} (G-modes, see Table SI-1, Supporting Information).

dx.doi.org/10.1021/jp312425m | *J. Phys. Chem. B* 2013, 117, 2221−2230

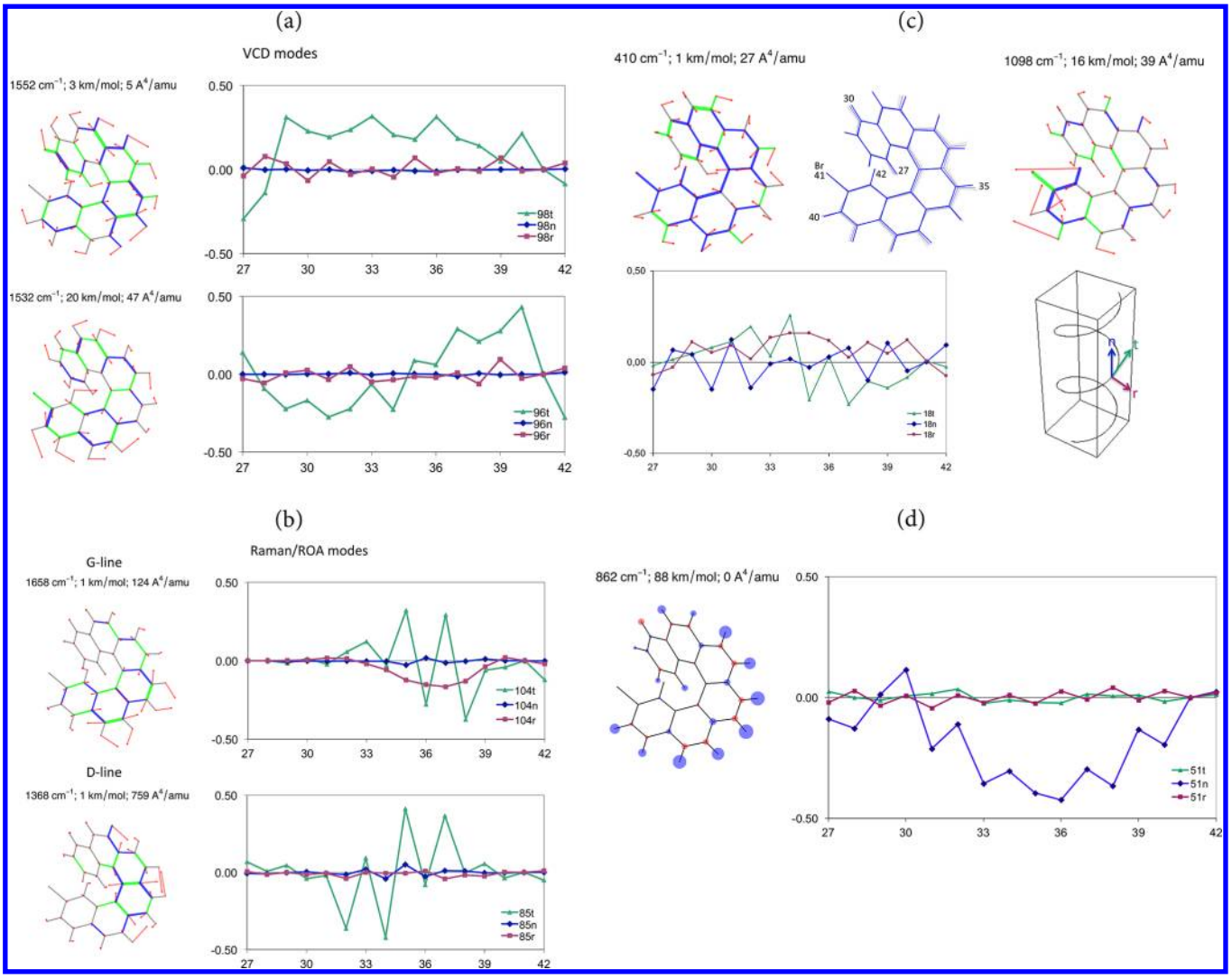

Figure 4. Sketch of selected nuclear displacements relevant for the ROA, Raman, IR, and VCD spectroscopy of 2-Br-hexahelicene (from DFT calculations). In parts a and b, we treat the important VCD and ROA G- and D-modes; in part c, we treat the ROA 410 cm^{-1} and IR C−Br stretching mode at 1098 cm^{-1}; in part d, we describe the IR 862 cm^{-1} mode (the size of blue/red circles of the molecular sketch are proportional to nuclear displacements in the out-of-plane direction). Red arrows represent displacement vectors; CC bonds are represented as green (blue) lines of different thickness according to their relative stretching (shrinking). For selected modes, we also report the hydrogen atom displacements, following ref 19 (for definitions of the **t**, **r**, and **n** axes, see part c of this figure).

Their representation also is provided in Figure SI-4 (Supporting Information). As reported in refs 42 and 43, one may see that, in each one of the three ranges, one has similar modes deriving from a common displacement pattern of the ring but with different phases: for this reason, in Figure 4A, we provide the description (also in terms of the approach introduced in ref 19) of just the most intense Raman or VCD modes, listed in Table 1.

Both the strong VCD and strong ROA modes (observed above 1300 cm^{-1}) are mixtures of HCC in-plane bending and skeletal CC stretching vibrations. For ROA, this had already been reported in ref 42, where it was admitted that the amplitude of the H atom's motion is large, due to the light mass of H, but does not cause large polarizability changes; we agree with this point of view and believe this is a general property of polyene and polyaromatic systems.[38] However, looking at the H motions (as reported in several panels in Figure 4) is helpful, since it allows easy characterization of the pattern of the nuclear motions along the helical structure. This is possible because of the coupling that exists between CH bending motions and vibrations of the polyaromatic molecular backbone.[48] The following observations can be made on this basis by comparing the two VCD and ROA NMs mentioned above (above 1300 cm^{-1}) (see Table 1 and Figures 3 and 4): (1) The two VCD NMs (corresponding also to the second strongest ROA modes in the high frequency range) are delocalized over all benzene units, while the two ROA NMs have more local character, notably the one with larger Raman activity extending over two or three central benzene units (see Figure 4A and B). (2) No C−Br stretching appears in any of the four modes.

Another interesting ROA mode is the one with a calculated frequency of 410 cm^{-1}: This is the symmetric combination of all the CC stretching coordinates in the inner and outer circles of hexahelicene, which can be described as a collective "acoustic-like" breathing of the whole helix. Similar Raman intense low-frequency acoustic-like vibrations are found in other sp^2 carbon materials, like nanotubes[49] and PAHs.[50] As for IR, the strongest feature is represented by the collective out-of-

dx.doi.org/10.1021/jp312425m | J. Phys. Chem. B 2013, 117, 2221−2230

plane CH bending mode computed at 862 cm^{-1}. This collective CH bending mode is a strong IR feature well-known and characteristic of aromatic compounds.[51] Interestingly, compared to the 862 cm^{-1} mode, the C−Br stretching mode computed at 1098 cm^{-1} is not particularly intense in IR as one might expect for a polar bond. This theoretical finding is consistent with the experimental IR spectra reported in Figure 5, where a comparison with DFT results is also provided. The description of the 410 and 862 cm^{-1} modes is provided in part B of Figure 4, in the same two ways as shown in part A.

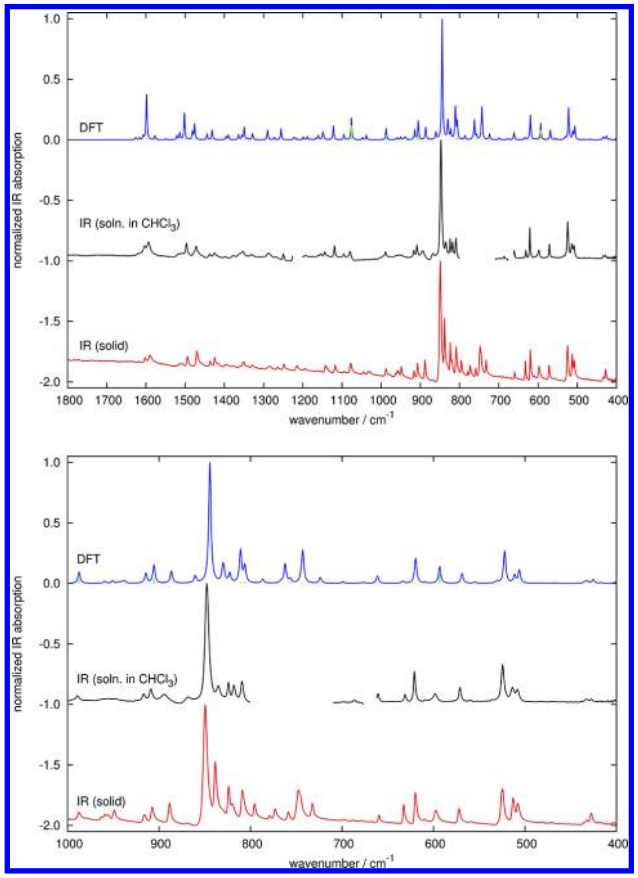

Figure 5. (top) Survey of the IR spectrum of 2-Br-hexahelicene in chloroform solution (black) and solid state (red) compared with DFT simulation (blue, wavenumber scaled by a factor of 0.98). For clarity, the normalized spectra are displayed offset. Green sticks represent the squared C−Br stretching content of the computed normal modes. (bottom) Zoom over the lower frequency region of the IR spectra. Interruptions in the solution state spectrum are due to saturation with solvent bands that prevents reliable subtraction.

The need to see whether there is any dependence of the data on the wavelength of the laser excitation and on the phase of the samples brought us to complete this work by recording the FT-Raman spectra (excitation at 1064 nm) both in the solid and in CH_2Cl_2 solution (Figure 6) and by running IR spectra (both in the solid and in solution, compared to theoretical data in Figure 5).

Very few differences are noticed in the Raman spectra in the solid and in solution (the latter data are slightly noisier, due to the lower concentration). Hence, the assumption that hexahelicene molecules in the solution or crystal phase do not interact strongly is tenable and justifies the assumption of running the DFT calculations for a single molecule. Even at

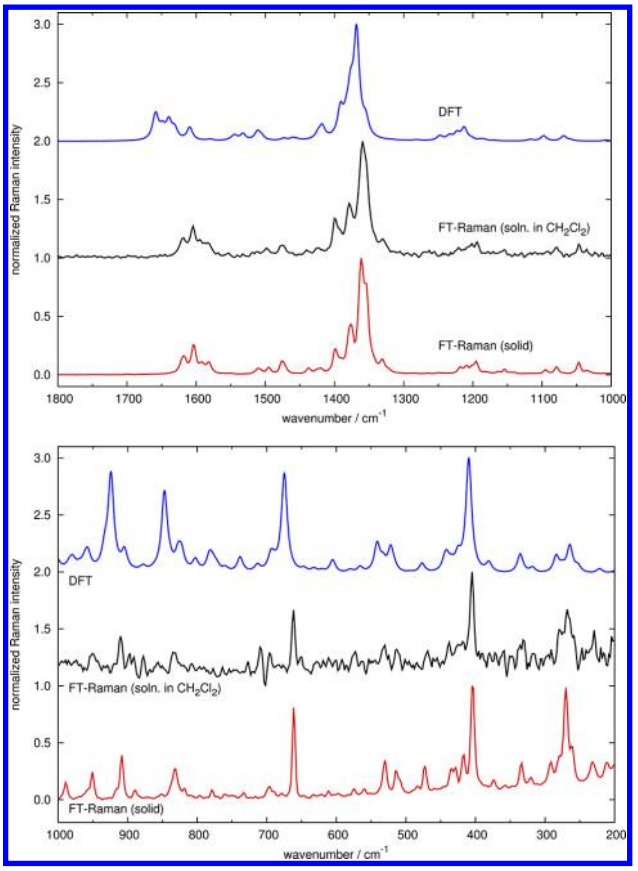

Figure 6. FT-Raman spectra of 2-Br-hexahelicene in solid state (red) and solution state (black line, CH_2Cl_2 bands have been subtracted). The top spectrum (blue) is obtained from DFT (Raman calculation in off-resonance conditions).

lower wavenumbers, this assumption provides calculated Raman spectra in good agreement with the experimental data, as may be seen in Figure 6. Also, in the IR, the correspondence between solid state and solution data and between single molecule calculations and experimental spectra is acceptable to a first approximation. However, comparing more carefully the spectra for solution and solid states reported in Figure 5, we notice clear intensity ratio differences in the frequency regions between 800 and 900 cm^{-1} and close to 500 cm^{-1}. This suggests that IR may be more sensitive a probe of intermolecular interactions in helicene samples; however, a more detailed investigation of this point is beyond the scope of the present work. The C−Br stretching mode is mostly involved in the NMs contributing insignificantly to IR, Raman, ROA, and even VCD activity; see, for instance, the stick plots overlaid on the spectral traces reported in the top of Figure 5 and in Figure SI-5 (Supporting Information).

We have also employed the results of the DFT calculations to generate a more detailed description of the molecular origin of the spectroscopic response, focusing on a readily available parameter directly related to the Raman intensity and used in the past for studying PAHs as prototypes of "graphitic" molecules.[48] This quantity, named α', is one-third the trace of the derivative of the molecular polarizability tensor with respect to a given stretching coordinate R, i.e., $\alpha' = {}^1/_3\,\mathrm{Tr}[d\boldsymbol{\alpha}/dR]$. As discussed in refs 38 and 48, the study of the α' parameters associated to the CC bonds of a polycyclic aromatic hydrocarbon nicely reveals how specific vibrational patterns

dx.doi.org/10.1021/jp312425m | J. Phys. Chem. B 2013, 117, 2221−2230

(notably the one associated with the strong Raman D-line, see Figures 3 and 4A) produce bond contributions adding constructively to the Raman intensity arising from the vibrating CC bonds.

Since it is possible to establish a connection between the normal modes of coronene and 2-Br-hexahelicene (see Figure 3 and ref 43), we expect that the Raman bond parameters α' are also related and can explain why only a few NMs provide good Raman signals in 2-Br-hexahelicene, coronene, and other PAHs: These modes are characteristic and selective. The plots reported in Figure 7 display a notable similarity both in

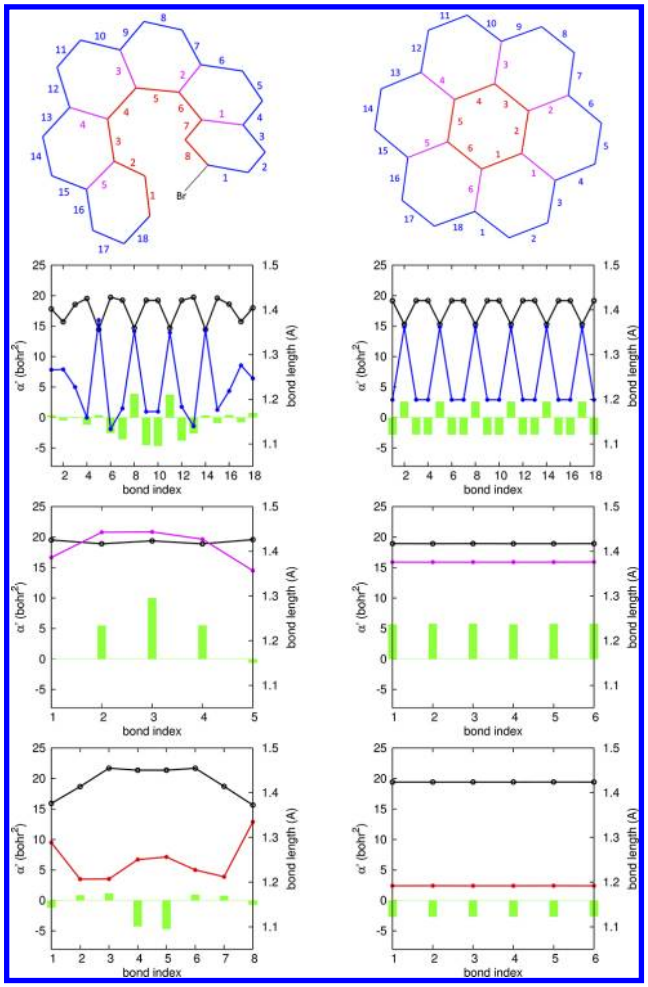

Figure 7. Plots of the Raman bond parameters α' for the set of CC bonds in 2-Br-hexahelicene (left) and coronene (right). The bond-numbering scheme is reported on the top. The bonds have been grouped in three sets associated to blue, magenta, and red colors. Every plot also reports the trends of the CC bond lengths (black line). The α' data reported for coronene compare well with previous DFT calculations.[48]

trends and α' values between coronene and 2-Br-hexahelicene, especially for the peripheral bonds of helicene (blue in Figure 7), involved in the strong Raman mode computed at 1368 cm^{-1} (see Figure 4A). Furthermore, it is worth noticing that the peculiar sawtooth pattern of the nuclear displacements along the peripheral bonds (see green histograms in Figure 7) appears rather localized on the central rings (radial bonds 3−4) of 2-Br-hexahelicene, while in coronene it is delocalized over the whole molecule. The inner and radial bonds of helicene (red and magenta in Figure 7) display somewhat larger differences in α' values with respect to coronene. Interestingly, the Raman activity of inner and radial bonds of 2-Br-hexahelicene is generally larger than in coronene, with the exception of radial bonds 1 and 5 and inner bonds 2, 3, and 7 for which the difference with coronene is small. Moreover, the α' values of the inner and radial bonds at the center of 2-Br-helicene correspond to local maxima, closely following the confined pattern of the nuclear displacements associated with the D-mode.

The data in Figure 7 shows the connection between the Raman intensity of the D-mode and the collective contributions from several CC bonds in 2-Br-hexahelicene. Neglecting contributions from other internal coordinates (which have been shown to be negligible in other PAHs[38,48]), one-third the trace of the molecular polarizability derivative ($^1/_3\, d\boldsymbol{\alpha}/dQ$) is given by the sum of the products of the nuclear displacements along CC stretchings (L_k) times the local bond parameters (α'_k): $^1/_3\, \mathrm{Tr}(d\boldsymbol{\alpha}/dQ) = \sum_k L_k \alpha'_k$. Visual inspection of Figure 7 reveals that the nuclear displacements are usually significant in correspondence with large α' values, thus explaining the rise in D-mode Raman activity. This is especially evident for the radial bonds. Overall, the pattern of α' values and nuclear displacements is such that the Raman activity of the D-mode computed for 2-Br-hexahelicene (760 A^4/amu) is not far from that computed for coronene (1272 A^4/amu). This is remarkable, since coronene, being planar, is in principle a more conjugated system; thus, it should exhibit a substantially larger Raman activity than 2-Br-hexahelicene (much more than a mere factor of 1.7 times). The analysis of the α' bond parameters and their comparison with coronene clearly reveals a similar magnitude and distribution in both molecules, hence explaining the reason why similar Raman intensities of the D-lines of the two molecules are found.

The behavior of CC bond lengths parallels that of α': Inspection of Figure 7 allows one to appreciate that a 1−2−1 pattern of alternated peripheral bonds (blue) both in 2-Br-hexahelicene and coronene takes place. This modulation is evident in the corresponding α' bond parameters. The radial bonds (magenta) are very similar in both molecules, while the inner ones (red) are substantially longer in 2-Br-hexahelicene due to the strained helical conformation. It is noticed that the behavior of the external CC stretchings is reminiscent of the alternation pattern described in 1D-conjugated conducting polymers and thus assigns a special role to the periphery of these 2D systems in supporting collective excitations. Interestingly, bond-length alternation patterns in PAHs can be directly measured now thanks to state-of-art AFM experiments.[52] Furthermore, we note that collective vibrational excitations have been discussed in the ROA context also for polypeptides.[53]

A similar relevance of the D-mode is noticed in the ROA experiment. However, in this case, some peculiar differences between coronene and 2-Br-hexahelicene are noticed in the behavior of $\partial\alpha^{zz}/\partial R$, with R being the stretching coordinates of the various CC bonds and z either the helix axis for 2-Br-hexahelicene or the axis perpendicular to the coronene plane (see Figure SI-6, Supporting Information). This provides a sensibly different polarizability tensor derivative for the D-mode, with enough dissymmetry to justify the intense ROA band (see Figure SI-7, Supporting Information). Indeed, the ROA intensity is due to the $\mathbf{G}'$ and $\mathbf{A}$ tensor derivatives, but from refs 22 and 34, it is clear that the latter tensor receive contributions from local $\boldsymbol{\alpha}$ tensor derivatives. In order to obtain

dx.doi.org/10.1021/jp312425m | J. Phys. Chem. B 2013, 117, 2221−2230

further insight into the unusual Raman and ROA activity of the D-mode of 2-Br-hexahelicene (computed at 1368 cm^{-1}) and to track the physical meaning of the α tensor, we have investigated with the TD-DFT method (TD-B3LYP/TZVP) the low lying singlet excitations and their coupling with vibrational NMs.

Among the first 10 excited states, one state in particular (S_3) stands out, possessing sizable oscillator and rotatory strengths (see Table 2). This fact grants contributions to both Raman and ROA activities arising from S_3, provided that a vibrational mode with a remarkable coupling to this state can be found. Therefore, we have computed the gradient at the Franck–Condon point (vertical transition) in correspondence with the S_3 potential energy surface. Indeed, the plot reported in Figure 8 indicates that the S_3 vertical gradient has a very similar pattern as that of the nuclear displacements of the D-mode computed at 1368 cm^{-1}. The electron–phonon coupling can be cast in a form involving the dot product of the gradient at the excited state surface and the normal mode nuclear displacements.[54] Hence, the similarity between Figure 8 and the nuclear displacements reported in Figure 3 suggests the existence of a good vibronic coupling between the S_3 excitation and the D-mode. This explains the good activity and selectivity in both Raman and ROA spectroscopies of the D-mode of 2-Br-hexahelicene.

Again, the situation in 2-Br-hexahelicene parallels that of coronene, where it has been shown[38,55] that the D-mode has a strong vibronic coupling with the lowest lying π–π^* excitation (mostly of HOMO–LUMO character). The outcome of our TD-DFT calculations on coronene (at the same level as those carried out on 2-Br-hexahelicene) agrees nicely with the previous analysis based on a semiempirical Hamiltonian for π electrons[55] (see the Supporting Information, Table SI-2 and Figure SI-8). For instance, the existence of this coupling was instrumental in explaining the Raman activity of the D-mode in coronene and many other PAHs.[38,55] However, what is essentially new in 2-Br-hexahelicene compared to coronene is that, due to the helical symmetry of helicene, the S_3 state also acquires a rotatory strength of R = 1.52 au in addition to its oscillator strength f = 0.28 (compare Table 2 and Table SI-2, Supporting Information). This promotes the activation of the D-mode in ROA spectroscopy.

Table 2. List of the 10 Lowest Energy Singlet States (S_n) of 2-Br-Hexahelicene Computed with the Time-Dependent DFT Method (TD-B3LYP/TZVP) and of Their Main Characteristics, Namely, Excitation Energy (or Wavelength), Oscillator, and Rotational Strengths[a]

S_n	$S_n - S_0$ (eV)	λ (nm)	oscillator strength (f)	rotatory strength (R, au)
1	3.2112	386.10	0.0079	0.0202
2	3.3678	368.14	0.0010	−0.0012
3[b]	**3.6180**	**342.69**	**0.2833**	**1.5213**
4	3.7115	334.05	0.0417	−0.1562
5	3.8804	319.51	0.0330	−0.0329
6	3.9460	314.20	0.0380	−0.0318
7	4.0631	305.15	0.0154	−0.0066
8	4.0953	302.74	0.0084	0.0379
9	4.1632	297.81	0.0189	−0.0237
10	4.2407	292.37	0.0117	0.0277

[a]The S_3 state (boldface) is characterized by substantial rotatory and oscillator strengths. [b]Orbitals involved in S_3 excitation (weights): HOMO-1 → LUMO (0.38949); HOMO-1 → LUMO+1 (0.22589); HOMO → LUMO (−0.13574); HOMO → LUMO+1 (0.50011).

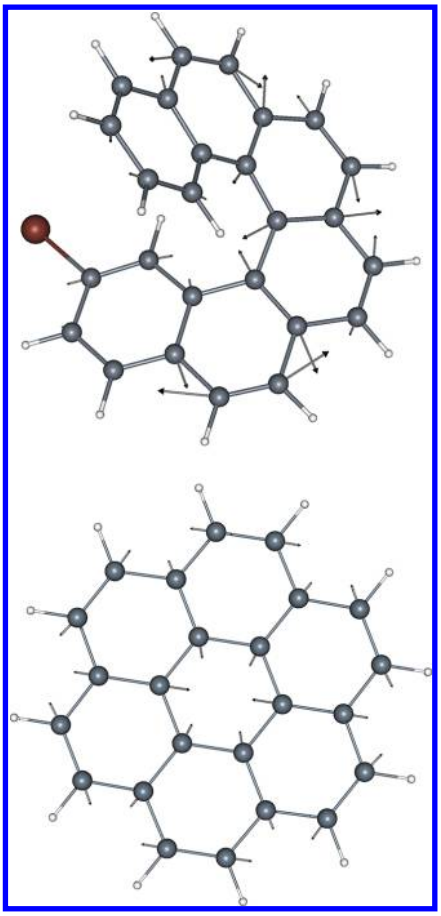

Figure 8. The gradient on the potential energy surface of excited state S_3 (with sign changed, so to represent atomic forces) of 2-Br-hexahelicene (top) and coronene (bottom). This has been computed with TDDFT at the Franck–Condon point (i.e. for a vertical excitation in correspondence with the ground state energy minimum). The pattern of the force vectors closely resembles the displacement vectors of the D-line strong Raman/ROA mode (see Figure 3).

SUMMARY AND CONCLUSIONS

In this work, we have measured the ROA spectrum of both enantiomers of 2-Br-hexahelicene. To the best of our knowledge, this had never been achieved for a simple helicene system. The interpretation of the data via DFT calculations for the isolated molecule results is fairly straightforward and, together with acquisition of IR and Raman spectra, demonstrates that the present ROA and Raman spectra are paradigmatic for helicene systems and (even) that vibrational modes show patterns typical of the ones reported in the literature[38] for graphene and PAH systems. In particular, the strongest ROA and Raman bands between 1350 and 1400 cm^{-1} associated with a combination of HCC in plane bending and CC deformation had been observed to occur in the Raman spectrum of coronene and other PAH systems with quite similar characteristics and had been called D-modes.[38]

The mean polarizability derivatives with respect to different types of CC stretching (external, radial, and internal), derived in tandem for 2-Br-hexahelicene and coronene on the basis of DFT, are shown to be important π-conjugation characteristics, which directly relate to other such properties like the CC bond

dx.doi.org/10.1021/jp312425m | J. Phys. Chem. B 2013, 117, 2221–2230

lengths and bond orders; the latter characteristics have been measured quite recently on hexabenzocoronene through the AFM technique[53] (a recent publication by Nakai et al. addresses similar issues based on analysis of CD spectra through TDDFT calculations[56]). We look forward to similar AFM measurements being made on analogous model systems for helicenes (e.g., pentabenzohexahelicenes) as well as on helicenes themselves, to evidence similarities and differences with respect to coronene and hexabenzocoronene. In this way, a clue to the understanding of similarities and differences between "curled" and "planar" PAH systems could be gained, as we have begun to do with the present study. Finally, we have tracked the special importance of D-modes and the reason of their strong Raman intensity, in the electron−phonon coupling of such modes, both in 2-Br-helicene and in coronene, with the strongest dipole allowed UV transition (S_3 excitation).

■ ASSOCIATED CONTENT

Supporting Information

HPLC chromatograms of 2-Br-hexahelicene derived from UV and CD detectors. Ball-and-stick representation of the *P* enantiomer of 2-Br-hexahelicene, as obtained from the optimized DFT structure. Comparison of the calculated Raman and ROA signals of α-pinene, β-pinene, and 2-Br-hexahelicene (computed with DFT methods). List of normal modes of 2-Br-hexahelicene relevant to Raman and ROA computed across the D- and G-band region by DFT. Representation of the nuclear displacements of the normal modes of 2-Br-hexahelicene. Low frequency region in FT-Raman/ROA of 2-Br-hexahelicene and C−Br stretching content of the NMs according to DFT calculations. Derivatives of the *zz*-component of the polarizability tensor ($\boldsymbol{\alpha}$) with respect to CC stretching coordinates in coronene and 2-Br-hexahelicene. Polarizability derivatives ($d\boldsymbol{\alpha}/dQ$) with respect to the normal coordinate (Q) of the D-mode in coronene and 2-Br-hexahelicene (from DFT calculations). List of the 10 lowest energy singlet states of coronene computed with the time-dependent DFT method (TD-B3LYP/TZVP). The gradient on the potential energy surface of excited state S_3 of coronene. This material is available free of charge via the Internet at http://pubs.acs.org.

■ AUTHOR INFORMATION

Corresponding Authors

*E-mail: abbate@med.unibs.it (S.A.).

*E-mail: matteo.tommasini@polimi.it (M.T.).

Author Contributions

C.J. and E.W.B.: ROA and Raman experiments and data interpretation. C.V.: HPLC and enantiomer separation and data interpretation. S.A. and G.L.: DFT calculations and data interpretation. N.R.A. and M.T.: Raman and IR experiments, DFT calculations, and data interpretation. D.A.L.: synthesis and data interpretation.

Notes

The authors declare no competing financial interest.

■ ACKNOWLEDGMENTS

E.W.B. and C.J. wish to acknowledge funding from the Biotechnology and Biological Sciences Research Council Tools and Resources Development Fund (BB/H023763/1) and the Engineering and Physical Sciences Research Council (EP/J019623/1). C.V. acknowledges financial support from MIUR-PRIN contract no. 20098SJX4F_004. S.A. and G.L. thank the Italian "Ministero dell'Istruzione, dell'Università e della Ricerca" (MIUR) for financial support, under the auspices of the PRIN program (2008 LYSEBR_003). M.T. and N.R.A. thank the Italian MIUR for financial support, under the auspices of the FIRB program RBFR08XH0H (Futuro in Ricerca 2008).

■ REFERENCES

(1) Martin, R. H. The Helicenes. *Angew. Chem., Int. Ed.* **1974**, *13*, 649−660.

(2) Starý, I.; Stará, I. G.; Alexandrová, Z.; Sehnal, P.; Teplý, F.; Saman, D.; Rulísek, L. Helicity Control in the Synthesis of Helicenes and Related Compounds. *Pure Appl. Chem.* **2006**, *78*, 495−499.

(3) Rybácek, J.; Huerta-Angeles, G.; Kollárovic, A.; Stará, I. G.; Starý, I.; Rahe, P.; Nimmrich, M.; Kühnle, A. Racemic and Optically Pure Heptahelicene-2-carboxylic Acid: Its Synthesis and Self-Assembly into Nanowire-Like Aggregates. *Eur. J. Org. Chem.* **2011**, 853−860.

(4) Lebon, F.; Longhi, G.; Abbate, S.; Gangemi, F.; Abbate, S.; Priess, J.; Juza, M.; Bazzini, C.; Caronna, T.; Mele, A. Chiroptical Properties of Some Monoazapentahelicenes. *J. Phys. Chem. A* **2004**, *108*, 11752−11761.

(5) Graule, S.; Rudolph, M.; Vanthuyne, N.; Autschbach, J.; Roussel, C.; Crassous, J.; Reau, R. Metal-bis(Helicene) Assemblies Incorporating pi-Conjugated Phosphole-Azahelicene Ligands: Impacting Chiroptical Properties by Metal Variation. *J. Am. Chem. Soc.* **2009**, *131*, 3183−3185.

(6) Katz, T. J. Syntheses of Functionalized and Aggregating Helical Conjugated Molecules. *Angew. Chem., Int. Ed.* **2000**, *39*, 1921−1923.

(7) Lovinger, A. J.; Nuckolls, C.; Katz, T. J. Structure and Morphology of Helicene Fibers. *J. Am. Chem. Soc.* **1998**, *120*, 264−268.

(8) Verbiest, T.; Van Elshocht, S.; Kauranen, M.; Hellemans, L.; Snauwaert, J.; Nuckolls, C.; Katz, T. J.; Persoons, A. Strong Enhancement of Nonlinear Optical Properties through Supramolecular Chirality. *Science* **1998**, *282*, 913−915.

(9) Passeri, R.; Aloisi, G. G.; Elisei, F.; Latterini, L.; Caronna, T.; Fontana, F.; Natali Sora, I. Photophysical Properties of N-Alkylated Azahelicene Derivatives as DNA Intercalators: Counterion Effects. *Photochem. Photobiol. Sci.* **2009**, *8*, 1574−1582.

(10) Moscowitz, A. On Optical Activity- Hexahelicene. Ph.D. Thesis, Harvard University, Cambridge, MA, 1957.

(11) Moscowitz, A. Theoretical Aspects of Optical Activity. Part One: Small Molecules. In *Advances in Chemical Physics*; Prigogine, I., Ed.; J. Wiley & Sons: New York, 1962; Vol. *IV*, pp 67−112.

(12) Rosenfeld, L. Quantenmechanische Theorie der Natürlichen Optischen Aktivität von Flüissigkeiten und Gasen. *Z. Phys.* **1928**, *52*, 161−174.

(13) Barron, L. D. Theoretical Rayleigh Optical Activity of Hexahelicene. *J. Am. Chem. Soc.* **1974**, *96*, 6761−6762.

(14) Barron, L. D. Theoretical Optical Rotation of Oriented Hexahelicene. *J. Chem. Soc., Faraday Trans. 2* **1975**, *71*, 293−300.

(15) Lightner, D. A.; Hefelfinger, D. T.; Frank, G. W.; Powers, T. W.; Trueblood, K. N. Absolute Configuration of Hexahelicene. *Nature (London)* **1971**, *232*, 124−125.

(16) Lightner, D. A.; Hefelfinger, D. T.; Frank, G. W.; Powers, T. W.; Trueblood, K. N. Hexahelicene. Absolute Configuration. *J. Am. Chem. Soc.* **1972**, *94*, 3492−3497.

(17) Hansen, A. E.; Bak, K. L. Ab-initio Calculations of Electronic Circular Dichroism. *Enantiomer* **1999**, *4*, 455−476.

(18) Furche, E.; Ahlrichs, R.; Wachsmann, C.; Weber, E.; Sobank, A.; Vögtle, F.; Grimme, S. Circular Dichroism of Helicenes Investigated by Time-Dependent Density Functional Theory. *J. Am. Chem. Soc.* **2000**, *122*, 1717−1724.

(19) Abbate, S.; Lebon, F.; Longhi, G.; Fontana, F.; Caronna, T.; Lightner, D. A. Experimental and Calculated Vibrational and Electronic Circular Dichroism Spectra of 2-Br-Hexahelicene. *Phys. Chem. Chem. Phys.* **2009**, *11*, 9039−9043.

(20) Nafie, L. A. *Vibrational Optical Activity – Principles and Applications*; Wiley: New York, 2011.
(21) Nafie, L. A.; Freedman, T. B. Vibrational Optical Activity Theory. In *Circular Dichroism Principles and Applications*; Berova, N., Nakanishi, K., Woody, R. W., Eds.; Wiley-VCH: New York, 2000; Chapter 4, pp 97–132.
(22) Barron, L. D. *Molecular Light Scattering and Optical Activity*; Cambridge Univ. Press: Cambridge, U.K., 1982; 2nd ed. thereof; Cambridge Univ. Press: Cambridge, U.K., 2004.
(23) Barron, L. D.; Hecht, L. Vibrational Raman Optical Activity: From Fundamentals to Biochemical Applications. In *Circular Dichroism Principles and Applications*; Berova, N., Nakanishi, K., Woody, R. W., Eds.; Wiley-VCH: New York, 2000; Chapter 23, pp 667–701.
(24) Barron, L. D.; Buckingham, A. D. Rayleigh and Raman Scattering from Optically Active Molecules. *Mol. Phys.* **1971**, *20*, 1111–1119.
(25) Vaccaro, P. H. Optical Rotation and Intrinsic Optical Activity. In *Comprehensive Chiroptical Spectroscopy*; Berova, N., Polavarapu, P. L., Nakanishi, K., Woody, R. W., Eds.; Wiley: New York, 2012; Vol. *1*, Instrumentation, Methodologies, and Theoretical Simulations, Chapter 11, pp 275–324.
(26) Polavarapu, P. L. Ab Initio Molecular Optical Rotations and Absolute Configurations. *Mol. Phys.* **1997**, *91*, 551–554.
(27) Polavarapu, P. L. Optical Rotation: Recent Advances in Determining the Absolute Configuration. *Chirality* **2002**, *14*, 768–781.
(28) Polavarapu, P. L. Ab Initio Vibrational Raman and Raman Optical Activity Spectra. *J. Phys. Chem.* **1990**, *94*, 8106–8112.
(29) Amos, R. D. Electric and Magnetic Properties of CO, HF, HCI, and CH3F. *Chem. Phys. Lett.* **1982**, *87*, 23–26.
(30) Brand, J. C. D.; Speakman, J. C. *Molecular Structure. The Physical Approach*, 2nd ed.; Halsted: New York, 1975; p 329.
(31) Barnett, J. C.; Drake, A. F.; Kuroda, R.; Mason, S. F. A Dynamic Polarization Model for Vibrational Optical Activity and the Infrared Circular Dichroism of a Dihydro[5]helicene. *Mol. Phys.* **1980**, *41*, 455–468.
(32) Abbate, S.; Havel, H. A.; Laux, L.; Pultz, V.; Moscowitz, A. Vibrational Optical Activity in Deuteriated Phenylethanes. *J. Phys. Chem.* **1988**, *92*, 3302–3311.
(33) Barron, L. D.; Clark, B. P. The Bond Polarizability Theory of Raman Optical Activity Calculations on (R) - (+) Bromochlorofluoromethane. *Mol. Phys.* **1982**, *46*, 839–851.
(34) Escribano, J. R.; Barron, L. D. Valence Optical Theory of Vibrational Circular Dichroism and Raman Optical Activity. *Mol. Phys.* **1988**, *65*, 327–344.
(35) Buckingham, A. D.; Longuet-Higgins, H. C. The Quadrupole Moments of Dipolar Molecules. *Mol. Phys.* **1968**, *14*, 63–72.
(36) Castiglioni, C.; Tommasini, M.; Del Zoppo, M. Experimental Vibrational Contributions to Molecular Hyperpolarisabilities: Methods and Measurements. *J. Mol. Struct.* **2000**, *521*, 137–155.
(37) Craig, D. P.; Thirunamachandran, T. *Molecular Quantum Electrodynamics*; Academic Press: London, 1984.
(38) Castiglioni, C.; Tommasini, M.; Zerbi, G. Raman Spectroscopy of Polyconjugated Molecules and Materials: Confinement Effect in One and Two Dimensions. *Philos. Trans. R. Soc. London* **2004**, *362*, 2425–2459.
(39) Xu, Z.; Gao, G. Graphene Chiral Liquid Crystals and Macroscopic Assembled Fibres. *Nat. Commun.* **2011**, *571*, 1–9.
(40) Hug, W. Measurement of Raman Optical Activity. In *Comprehensive Chiroptical Spectroscopy*; Berova, N., Polavarapu, P. L., Nakanishi, K., Woody, R. W.; Wiley: New York, 2012; Vol. *1*, Chapter 6, pp 147–178.
(41) Frisch, M. J.; Trucks, G. W.; Schlegel, H. B.; Scuseria, G. E.; Robb, M. A.; Cheeseman, J. R.; Scalmani, G.; Barone, V.; Mennucci, B.; Petersson, G. A.; et al.; *Gaussian 09*, revision A.02; Gaussian, Inc.: Wallingford, CT, 2009.
(42) Liégeois, V.; Champagne, B. Vibrational Raman Optical Activity of π-Conjugated Helical Systems: Hexahelicene and Heterohelicenes. *J. Comput. Chem.* **2009**, *30*, 1261–1270.
(43) Thomsen, C.; Machón, M.; Bahrs, S. Raman Spectra and DFT Calculations of the Vibrational Modes of Hexahelicene. *Solid State Commun.* **2010**, *150*, 628–631.
(44) Merten, C.; Barron, L. D.; Hecht, L.; Johannessen, C. Determination of the Helical Screw Sense and Side-Group Chirality of a Synthetic Chiral Polymer from Raman Optical Activity. *Angew. Chem., Int. Ed.* **2011**, *50*, 9973–9976.
(45) Barron, L. D.; Hecht, L.; Gargaro, A. R.; Hug, W. Vibrational Raman Optical Activity in Forward Scattering: Trans-Pinane and β-Pinene. *J. Raman Spectrosc.* **1990**, *21*, 375–379.
(46) Kubala, D.; Drage, E. A.; Al-Faydhi, A. M. E.; Kocisek, J.; Pappa, P.; Matejcik, V.; Mach, P.; Urban, J.; Limão-Vieira, P.; Hoffmann, S. V.; Matejcik, S.; Mason, N. Electron Impact Ionisation and UV Absorption Study of α- and β-Pinene. *Int. J. Mass Spectrom.* **2009**, *280*, 169–173.
(47) Luber, S.; Reiher, M. Intensity-Carrying Modes in Raman and Raman Optical Activity Spectroscopy. *ChemPhysChem* **2009**, *10*, 2049–2057.
(48) Negri, F.; Castiglioni, C.; Tommasini, M.; Zerbi, G. A Computational Study of the Raman Spectra of Large Polycyclic Aromatic Hydrocarbons: Toward Molecularly Defined Subunits of Graphite. *J. Phys. Chem. A* **2002**, *106*, 3306–3317.
(49) Dresselhaus, M. S.; Dresselhaus, G.; Avouris, Ph. *Carbon Nanotubes*; Springer: Berlin, 2001.
(50) Di Donato, E.; Tommasini, M.; Fustella, G.; Brambilla, L.; Castiglioni, C.; Zerbi, G.; Simpson, C. D.; Müllen, K.; Negri, F. Wavelength-Dependent Raman Activity of D2h Symmetry Polycyclic Aromatic Hydrocarbons in the D-Band and Acoustic Phonon Regions. *Chem. Phys.* **2004**, *301*, 8193.
(51) Jones, R. N.; Sandorfy, Ca. The Application of Infrared and Raman Spectrometry to the Elucidation of Molecular Structure. *Chemical Applications of Spectroscopy-Techniques of Organic Chemistry*; Wiley: New York, 1956; Vol. *9*.
(52) Gross, L.; Mohn, F.; Moll, N.; Schuler, B.; Criado, A.; Guitián, E.; Peña, D.; Gourdon, A.; Meyer, G. Bond-Order Discrimination by Atomic Force Microscopy. *Science* **2012**, *337*, 1326–1329.
(53) Profant, V.; Baumruk, V.; Li, X.; Šafařík, M.; Bouř, P. Tracking of the Polyproline Folding by Density Functional Computations and Raman Optical Activity Spectra. *J. Phys. Chem. B* **2011**, *115*, 15079–15089.
(54) Tommasini, M.; Castiglioni, C.; Zerbi, G. Raman Scattering of Molecular Graphenes. *Phys. Chem. Chem. Phys.* **2009**, *11*, 10185–10194.
(55) Negri, F.; Di Donato, E.; Tommasini, M.; Castiglioni, C.; Zerbi, G.; Müllen, K. Resonance Raman Contribution to the D Band of Carbon Materials: Modeling Defects with Quantum Chemistry. *J. Chem. Phys.* **2004**, *120*, 11889–11900.
(56) Nakai, Y.; Mori, T.; Inoue, Y. Theoretical and Experimental Studies on Circular Dichroism of Carbo[n]helicenes. *J. Phys. Chem. A* **2012**, *116*, 7372–7385.